Characterization of Advective Micromolding in Vapor-Permeable Templates for Printed Electronics

John Herr
Albert Pisano, Ed.

Electrical Engineering and Computer Sciences
University of California at Berkeley

Technical Report No. UCB/EECS-2015-149
http://www.eecs.berkeley.edu/Pubs/TechRpts/2015/EECS-2015-149.html

May 19, 2015

Acknowledgement

I would like to take this opportunity to thank my research adviser, Professor Albert Pisano, for his support of me on this project. I am thankful for the opportunities he has provided during my time working with him and his persistent optimism that has helped me to see this project through to completion.

I am also very thankful to all the members of the Pisano Research for Integrated Micromechanical & Electrical (PRIME) Systems Laboratory for insight on this project. I specifically would like to thank David Rolfe and Kristen Dorsey for introducing me to this printing process and providing technical guidance when it was needed.

Lastly, I am very grateful for Professor Liwei Lin’s support on this project. Without the use of facilities this project would not have been possible.

Characterization of Advective Micromoding in Vapor-Permeable Templates for Printed Electronics

JOHN HERR

May 2015

Submitted to the Department of Electrical Engineering and Computer Sciences, University of California at Berkeley, in partial satisfaction of the requirements for the degree of Master of Science, Plan II.

Approval for the Report and Comprehensive Examination:

Committee:

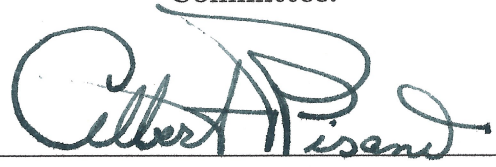

Professor Albert Pisano
Research Advisor

18 MAY 2015

(Date)

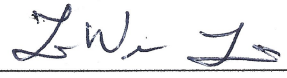

Professor Liwei Lin
Second Reader

5/18/2015

Abstract

Significant efforts have been made in recent years to develop new patterning methods for printed sensors and electronics that are simpler and allow for new materials to be patterned compared to traditional fabrication processes. One newly conceived patterning method is the use of advective micromolding in vapor-permeable templates (AMPT) [1]. AMPT is a single-step additive patterning process that uses permeation pumping to pattern and concentrate a nanoparticle ink inside a permeable template, resulting in close-packed nanoparticle features. This process can be performed at low pressure and temperature, and is compatible with printing materials such as nanoparticles and polymers that can be difficult to print with other methods.

In this work, models are presented for printing conductors, capacitors, resistors, as well as passive low-pass filters. Using ink composed of 20nm silver nanoparticles suspended in ethanol and templates made from PDMS, these basic components were patterned using AMPT and thermally sintered. Printed devices were then characterized for use in printed electronics.

Acknowledgements

I would like to take this opportunity to thank my research adviser, Professor Albert Pisano, for his support of me on this project. I am thankful for the opportunities he has provided during my time working with him and his persistent optimism that has helped me to see this project through to completion.

I also have very thankful to all the members of the Pisano Research for Integrated Micromechanical & Electrical (PRIME) Systems Laboratory for insight on this project. I specifically would like to thank David Rolfe and Kristen Dorsey for introducing me to this printing process and providing technical guidance when it was needed.

Lastly, I am very grateful for Professor Liwei Lin's support on this project. Without the use of facilities this project would not have been possible.

Contents

Abbreviations

AMPT	**A**dvective **M**icromolding in Vapor-**P**ermeable **T**emplates
CVD	**C**hemical **V**apor **D**eposition
DI	**D**e **i**onized water
DOS	**D**ensity **O**f **S**tates
EHD	**E**lectro**h**ydro**d**ynmaic
HMDS	**H**exa**m**ethyl**di**s**i**lazane
IPA	**I**so**p**ropyl **A**lcohol
KOH	Potassium Hydroxide
MEMS	**M**icro **E**lectrical **M**echanical **S**ystems
MM	**M**icro **M**olding
MMIC	**M**icro **M**olding **I**n **C**apllaries
NIL	**N**ano **I**nprint **L**ithography
PECVD	**P**lasma **E**nhanced **C**hemical **V**apor **D**eposition
PDMS	**P**oly(**dim**ethal**s**iloxane)
PMP	**P**oly(4-**m**ethyl-2-**p**entyne)
RIE	**R**eactive **I**on **E**tch)
SAMIM	**S**olvent **A**bsorption **Mi**cro**m**olding
UV	**U**ltra **V**iolet

Symbols

A	Cross Sectional Area	μm^2
C	Capacitance	F
$c_{1,2,3,4}$	Coefficients for Current Sheet Expression	
d	Spiral diameter for inductors	μm
$K_{1,2}$	Coefficients for Modified Wheeler Expression	
L	Inductance	H
n	Number of inductor turns	
Q	Quality factor	μm
s	Turn/Finger spacing for inductors/capacitors	μm
t	Dielectric Thickness	μm
w	Width	μm
Δ	Inductor Fill ratio	
ϵ_0	Vacuum Permittivity	8.854E-12 F/m
ϵ_r	Relative Permittivity / Dielectric Constant	
μ_0	Permeability of Free Space	$4\pi \cdot 10^{-7} \frac{N}{A^2}$
ω	Angular Frequency	$\frac{rad}{s}$
ω_{break}	Cutoff Frequency	$\frac{rad}{s}$
ρ	Resistivity	$\frac{\Omega}{m^2}$

Chapter 1

Introduction and Background

1.1 The Demand for Microfabrication Development

The explosive development of miniaturized circuitry for sensors and portable electronics in recent years has led to a world that is becoming increasingly more connected. In todays informational age there is a continual demand for the improvement of sensors that fuel our internet of things. By aggregating data from a wide variety of sources we are finding new ways to improve the value, functionality, and efficiency of devices and systems.

Over the past few decades this demand for data has fueled significant improvements in the size, cost, size, accuracy, and robustness of sensors. Improvements have been made while continuing to rely on traditional fabrication processes that are limited to using the bulk semiconductor materials such as silicon and gallium arsenide. While traditional fabrication processes have continued to yield improvements in sensor technology, it is likely that future improvement will lie in the development of alternative fabrication techniques and the increased material set they allow to be provided.

This work focuses on the characterization of a template-based method for nanoparticle printing. If this process can be further developed into a roll-to-roll patterning system it may provide cost advantages over current fabrication methods. To provide background and context to this work a brief review of traditional patterning methods. A description of the AMPT patterning method will be provided along with the motivation and goal of this work.

1.2 Traditional Microfabrication

Traditional microfabrication refers to industry standard processes that rely primarily on photolithography as a means of patterning devices. Traditional microfabrication processes are extremely well characterized having been developed and improved upon over the last fifty years with the growth of the integrated circuit industry. These processes can be grouped into two major categories, bulk micromachining and surface micromachining. Surface micromachining is when features are built on top of a substrate wafer by deposition and etching of additional structural layers. In contrast, bulk micromachining is when features are created by selectively etching a substrate wafer. While traditional microfabrication processes have proved be effective at producing high-resolution devices, ideas for printed electronics using new materials are often incompatible with the traditional processes briefly described here.

1.2.1 Patterning

Traditional processes rely on photolithography to produce fine features on surfaces. In photolithography, polymeric optically-sensitive materials, referred to as photoresists or more simply resists, are first deposited on a wafer by spin casting. After spin casting, a wafer undergoes a low temperature bake to remove the solvent and solidify the resist. A wafer is then ready to undergo the exposure process shown in Figure 1.1. A photomask containing transparent and opaque regions that define the two dimensional geometry of the pattern to be transcribed is then brought in contact with the wafer. Ultraviolet light is directed through the photomask exposing the resist under the transparent portion of the mask resulting in a change of the chemical properties of the resist to make them soluble or insoluble. After exposure, a wafers are chemically washed with a developer removing the soluble portion of the resist and the remaining patterned resist is baked again to form a hardened more chemically inert layer [2]. Positive resists are insoluble to developer until they are exposed with ultraviolet light and become soluble. Conversely, negative resists are soluble until they are expose to UV light, inducing cross-linking, and making the resist insoluble.

There are several variations of photolithography that are commonly used to push the achievable resolution with this process. Using a stepper, lenses are used to downsize the

pattern transmitted in a mask. In immersion photolithography, air is replaced by a fluid with a refractive index greater than 1 to slow light down and enhance resolution. When e-beam lithography is performed, electrons with a high enough energy are selectively fired a to achieve the same effect of high energy light in a photoresist layer.

Using extreme UV photolithography a 25 nm 1:1 line/space resolutions with a line edge roughness of less than 3 nm[3] can be achieved. While photolithography has been perfected over the years, it has drawbacks. To pattern features with a high yield rate an ultra clean environment is required as small dust particles can easily ruin a patterned device. Photolithography is also typically limited use with commonly used wafer substrates, like crystalline silicon, where photoresist adhesion issues have been mitigated by the addition of thin films such as HMDS, and exposure settings have been well characterized. High temperature baking processes and chemical washes required during photolithography also make this process incompatible with certain materials.

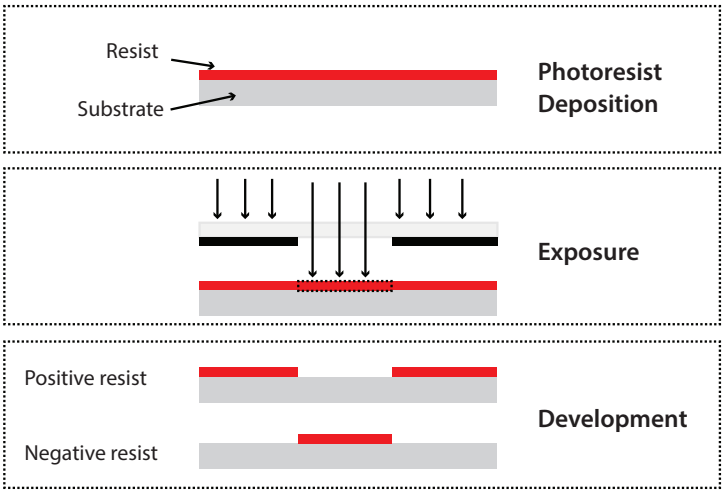

FIGURE 1.1: The standard photolithography process

1.2.2 Additive and Subtractive Processes

Resists, such epoxy-based SU-8, can be used as structural materials, however resists are typically used to as a sacrificial layers to transcribe the patterns into yet another layer. Figure 1.2 illustrates the major classifications of traditional additive and subtractive processes.

Additive processes are classified as being the result of a chemical reaction (CVD, electrodeposition, epitaxy, thermal oxidation) or as the result of a physical reaction (evaporation, sputtering, casting). These results can be either conformal as in the case of CVD, or non-conformal as in the case of evaporation where the added material is being projected from a point source.

Subtractive processes are labeled as being isotropic etches, anisotripic etches, or lift-off steps. Isotropic etches are chemical etches that etch evenly in all directions undercutting a masking layer while isotropic etches etch in a particular direction as in the case of a RIE or a wet etch of silicon with KOH. Etch steps are material specific and have a selective etch rate against the masking material.

While each material can only be deposited or etched with a subset of these standardized processes, these process become even constricting when considering a complete process flow as a result of thermal and material property constraints. Metals, photoresists, and polymer films are incompatible with subsequent high temperature processing steps. In certain circumstances there are lower temperature processes that can be substituted for a high temperature ones, such as when PECVD is used to replace LPCVD to deposit a dielectric film. In this case a lower deposition temperature can be had, but only at the cost producing a low-grade film with a high void content that is more easily etched. The temperatures involved in these steps also have a profound effect in residual thin film stresses and can result in increase dopant diffusion, and changes in the morphology of polycrystalline materials.

While nanoparticles have been patterned using thin film deposition and etching [4], the accumulated restriction of each process in the entire process flow of a device limits the uses of tradition microfabricaiton to a small set of materials.

1.3 Alternative Patterning Methods

In this section several of the more common alternative patterning methods are reviewed. Alternative patterning methods differ from traditional microfabrication in that photolithography and e-beam lithography are not used as a primary means of patterning.

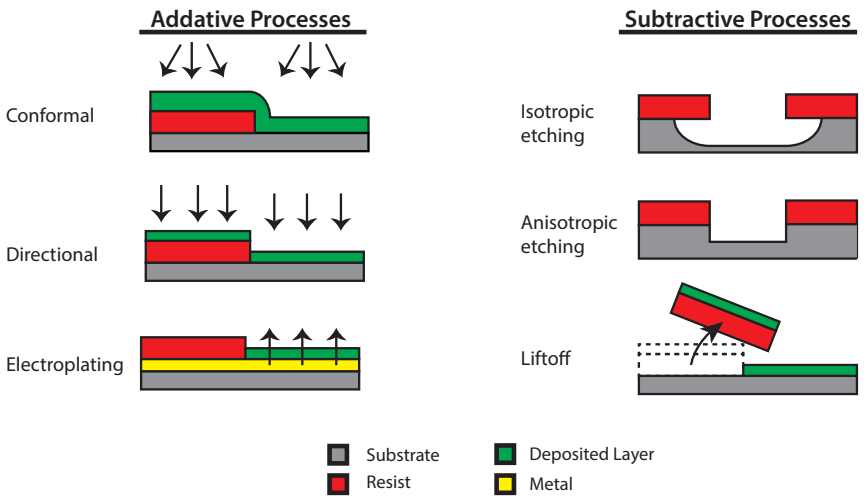

FIGURE 1.2: The result of traditional additive and subtractive processes.

The development of these alternative methods has been stimulated by goals to increase the use of the limited material set allowed for using traditional fabrication. Most notably, alternative methods have been pushing the boundaries of what is possible to make with nanoparticles and polymers.

The ability to pattern nanoparticles is of significant interest because nanoparticles posses significantly different material properties than their bulk counterparts due to a higher surface to volume ratio and quantum effects[5]. As nanoparticles decrease in size, electrical and optical properties are significantly affected as these properties depend on the crystals band structures and density of states (see Figure 1.3). Due to these properties there has developed a need to pattern nanoparticles for biosensors [6], catalysts [7], photonics [8], low temperature metal electrode deposition, , gas sensors [9], and other MEMS applications [10].

Polymers are large molecules consisting of repeating units that determine their electrical, physical, and chemical properties. Conjugated polymers, consisting of altering single and double bonds in the backbone, can be doped to be conductive and are used in a variety of electronic sensors [11]. Polymers can also swell in response to chemicals making them useful for sensing applications and their low cost makes them useful as a structural or encapsulation materials [12].

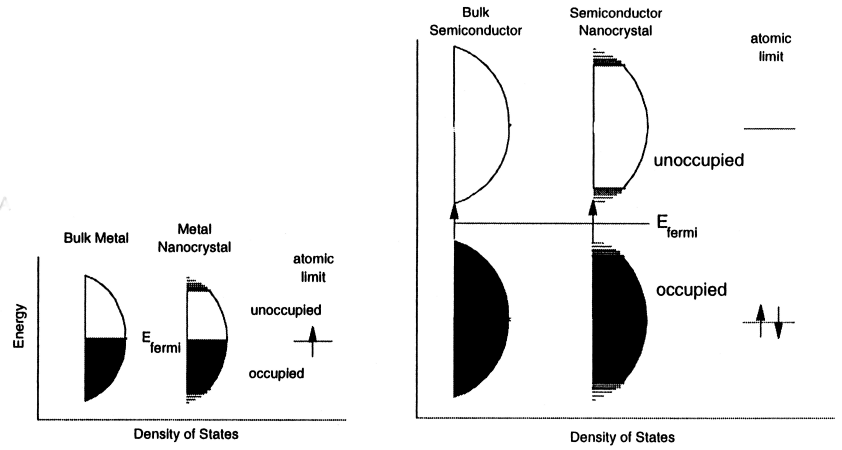

FIGURE 1.3: Nanocrystals have unique electrical and optical properties due to a DOS that lies between that of an atom and bulk material. Here the DOS is shown for a metal (left) and a semiconductor (right) [5]

1.3.1 Inkjet-Based Patterning

Inkjet printing might be the most commonly used method for patterning polymers and nanoparticles in part because it is a completely additive process eliminating the need for etching to define features. In this process droplets of ink are ejected from a nozzle on to a substrate typically by thermal or piezoelectric actuation [13]. Patterning is achieved when the nozzle above the substrate is moved in a controlled manner to selectively place droplets of ink that solidify by evaporation or a UV exposure to form solidified features.

While inkjet printing is used for many applications, the process highly dependent on the fluidic properties of the ink being used and the surface properties of the substrate. Unless an array of nozzles is used, device throughput is typically very low. Since features are formed from an agglomeration of ink droplets feature resolution is limited to being larger than 20 μm. Further, because this is a fluidic based process only thin films can be created with aspect ratios limited to roughly 1:10 [14].

Electrospinning and Electrodynamic (EHD) printing are adaptations of inkjet printing that allow for finer resolution. In these processes an electric potential is applied between the nozzle and the substrate that creates an electrically driven continuous jet (electrospinning) or a stream of discreet droplets (EHD). Because of the forces at the fluid-air interface a Taylor cone is created in which produces drops with smaller dimensions than could otherwise be created [15].

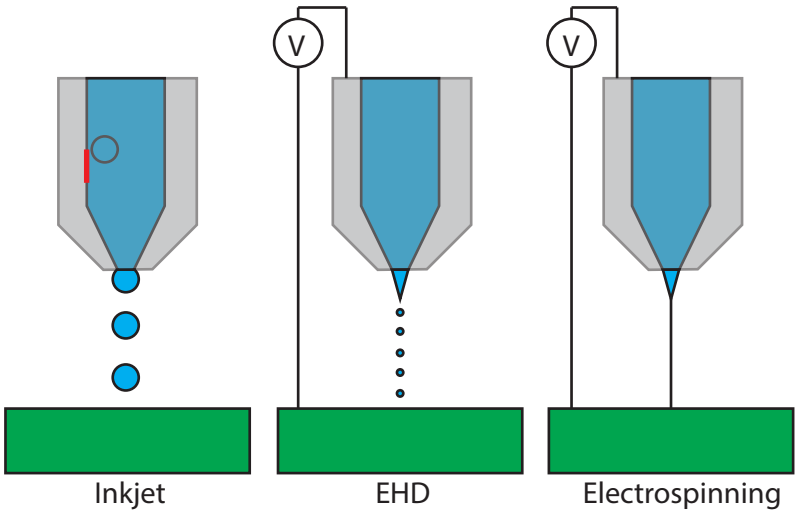

FIGURE 1.4: Inkjet patterning processes

1.3.2 Rigid Template Patterning

Rigid template patterning methods include gravure, screen-printing, and nanoimprint lithography. Unlike inkjet printing where patterning is controlled thorough movement of the nozzle, in template-based methods features are formed when ink is constrained to the geometry of the template and then solidified.

Gravure printing for nanoparticles and polymers has been adapted from the process used to print magazines, wallpapers, and food packaging. In this process a form roller with the pattern engraved is inked and rolled across the substrate. The ink is then transferred to the substrate and where it reflows and solidifies forming the final features as the solvent in the ink evaporates [16]. Pattern quality is dependent on the engraving quality of the form roller, fluidic properties of the ink suspension, and surface properties of the substrate. If the ink does not fully fill features or if there is excess ink on the form roller that is not removed by the wiping blade features will not pattern properly. Gravure printing has been successfully used for patterning of nanoparticles[17] and polymers[18] for simple electrical components. Due to reflow of ink after it is on the substrate features sizes must be larger than 20 μm [19] and aspect ratios are typically less than 1:4 [20].

Like gravure patterning, screen printing (shown in Figure 1.6) is a long-standing industrial process that has recently been adapted for patterning nanoparticles and polymers.

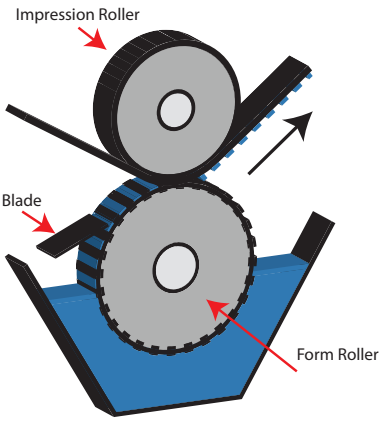

FIGURE 1.5: Gravure printing process

In this process ink is forced through a screen stencil when a rubber squeegee moves along the surface of the screen, defining the pattern. With screen printing a number of devices have been demonstrated including transistors [21], gas sensors, biosensors [22] and energy harvesting devices [23]. Similar to gravure printing, reflow of ink on the surface of the substrate limits minimum feature sizes and aspect ratios are low, typically less than 1:4 [24].

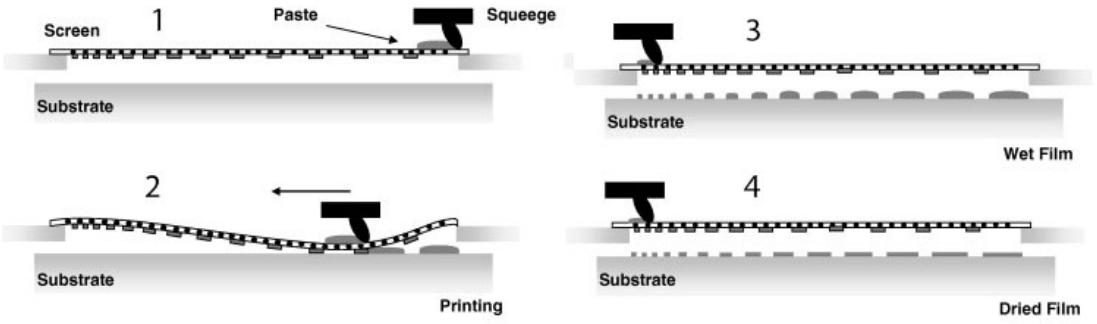

FIGURE 1.6: Screen-printing process [25]

A third form of rigid template patterning is nanoimprint lithography (NIL) (Figure 1.7). As the name implies NIL can produces high quality features with straight edges and is capable of finer resolution than inkjet or screen printing methods having been shown to pattern polymers with feature sizes of characteristic dimensions less than 10 nm [26]. With rigid NIL, patterned materials are primarily liquid polymers containing a UV or thermally activated cross-linkers, or thermoplastic polymers above their glass transition temperatures [27]. Due to the changing rheology of nanoparticle ink under the pressure of the template, it is not well suited for this process.

In this process the material being pattered is deposited onto the substrate, and then the template is lowered onto the substrate and pressed forming the features. The patterned material is then solidified and the template is removed. Since ink being patterned has no place to escape during the imprinting process, a chemical or plasma etch is typically required to remove the residual layer between features [28].

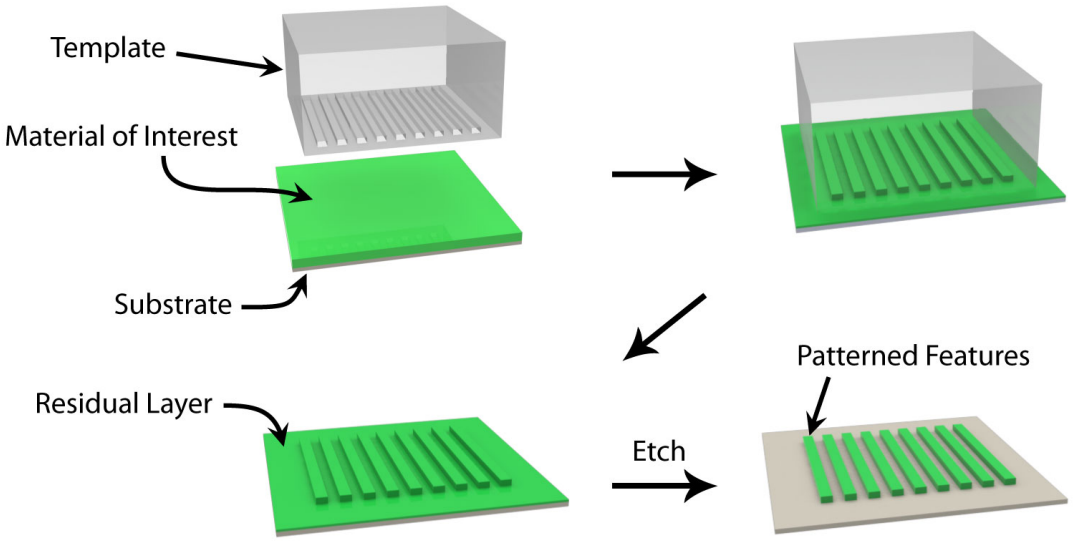

FIGURE 1.7: Nanoimprint lithography process [27]

1.3.3 Soft Template Patterning

Soft nanoimprint lithography has the same procedure as NIL (Figure 1.7), except a flexible templates such as PDMS is used. Being soft, these templates have a low Young's modulus and often swell due to solvent saturation. If swelling occurs features will become distorted during the imprinting process [29]. Because of swelling, the residual layer can also have varying thickness further complicating the etching process. Using soft templates, NIL has been able to produce features with line widths less than 100 nm [27].

When solidification is a result of solvent evaporation thought the template in soft nanoimprint lithography, the process is called solvent absorption micromolding (Figure 1.8). A variation of this process for patterning polymers is solvent assisted micromolding. In this process a polymer is spin casted onto a wafer and pressed against a template coated with a solvent that dissolves the polymer locally in the defined regions of

the template leaving the polymer with the patterned geometry upon solidification. Solvent assisted and solvent absorption micromolding have been used to pattern polymers [30] and nanoparticles [31].

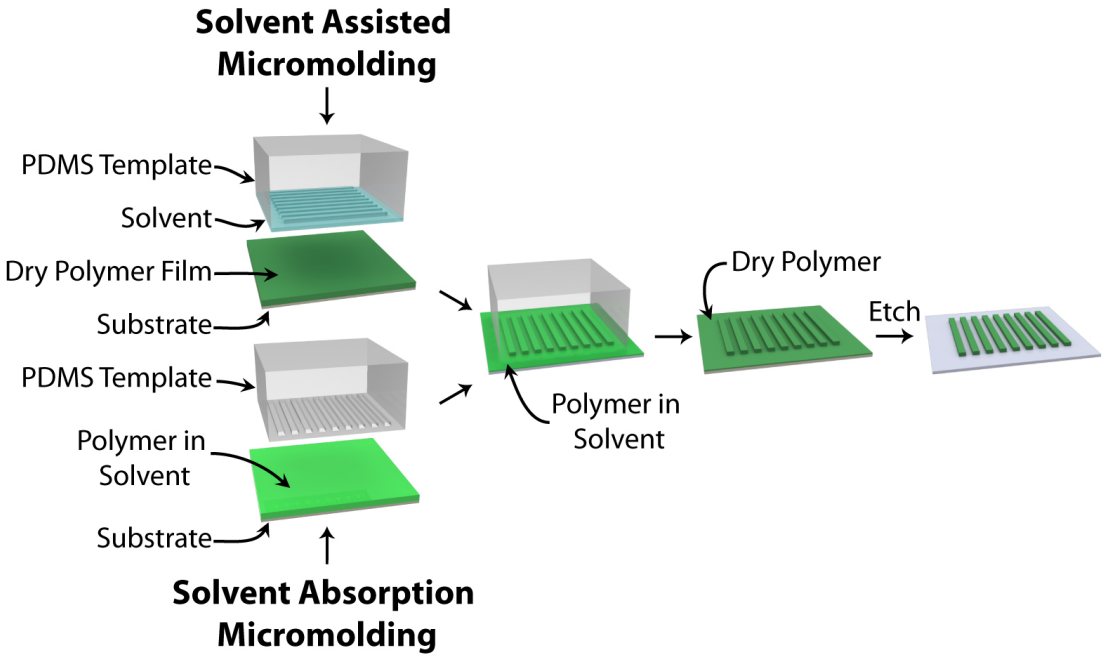

FIGURE 1.8: Solvent assisted and solvent absorption micromolding processes [27]

Micromolding in capillaries (MIMIC) is printing system for polymers that is based on capillary forces (Figure 1.9). A soft permeable template, typically PDMS, with channels reaching the edge of the template mold is first pressed onto the substrate. Liquid polymer ink is then deposited on the edge of the template where openings to the channels are located. Capillary forces pull the liquid polymer into the channels as air escapes through the permeable template. Once channels are filled, polymer ink is solidified through a cross-linking step and the template is removed. Using MIMIC lines as small as 300 nm [32] and height to width aspect ratios as high as 1:1 [33] have been demonstrated. As with soft NIL, the required pressure on the template typically results in deformation of the intended feature geometry. Further, if a template consists of lengthy small channels, features may take a long time to fill [34].

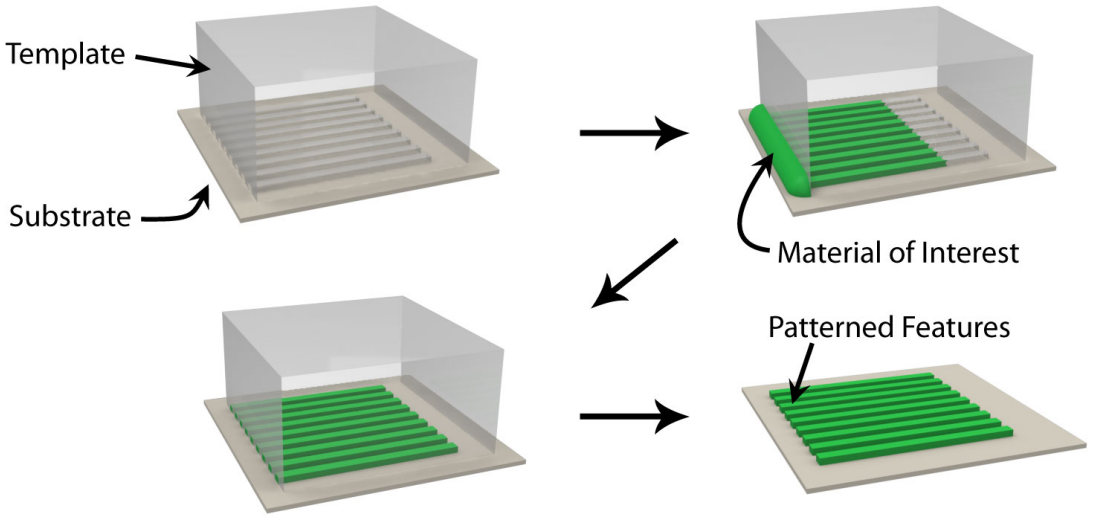

FIGURE 1.9: Micromolding in Capillaries [27]

1.4 Advective Micromolding in Vapor-permeable Templates (AMPT)

The work of this report pertains to the soft template patterning process depicted in (Figure 1.10. Like solvent assisted and solvent absorption micromolding, ink is solidified in AMPT as a result of solvent evaporating through a template. AMPT differs from these processes though in that it is completely additive, eliminating material incompatibilities brought about by a residual layer etches.

In the AMPT printing process a layer of clean solvent is first deposited on the substrate that is to be patterned. A permeable template such as PDMS or PMP is placed onto the substrate such that the clean solvent fills the features of the template completely. Sufficient pressure is applied such that the soft mold conforms to the substrate. Any solvent that happens to be trapped between the substrate and non-patterned area evaporates through the template leaving solvent only in the engraved template features. Nanoparticle or polymer ink is then added to templates vias that are accessed from the template edges, and a heater is used to increase solvent evaporation through the template. As solvent evaporates, a pressure gradient draws ink into the channel where it self-concentrates forming the patterned features. Once no solvent remains, the template can be removed. After removing the template steps such as sintering metal nanoparticles can then be performed to alter the properties of the patterned material.

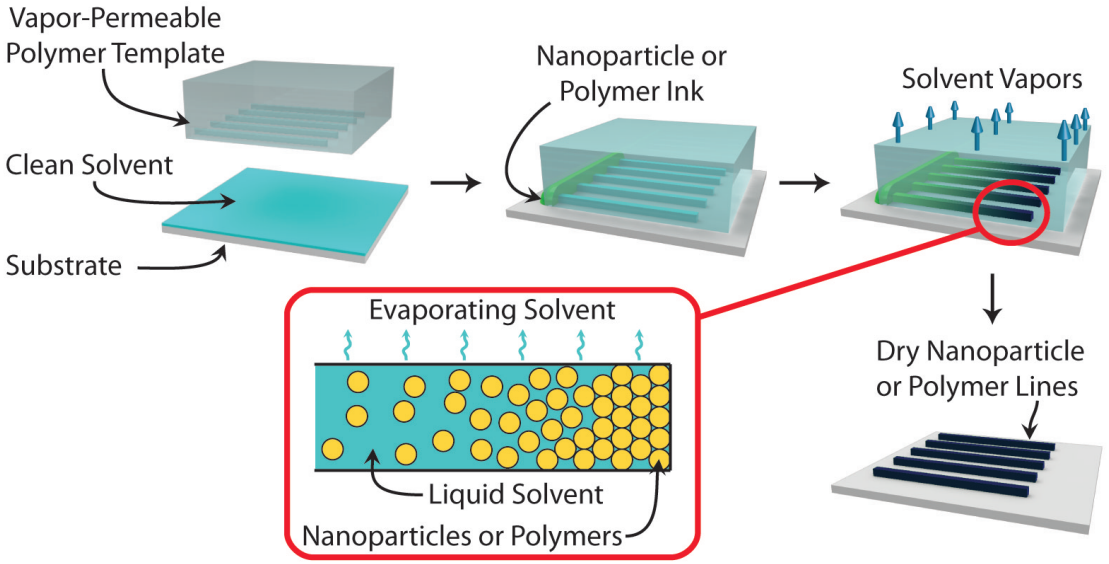

FIGURE 1.10: AMPT printing process [27]

1.5 Motivation and Outline

AMPT is a new printing process that has potential to be further developed into an extremely versatile process. Since temperatures are kept low, typically $\approx 40 - 50°C$, this process mitigates unwanted effects such as diffusion of doped materials and allows for patterning on substrates that have low melting temperatures. As the process is purely additive there are no etching steps that might damage important structures on a device. By using clean solvent to prefill the template, the dependence on surface interactions between the ink and the substrate that are limiting in MMIC are eliminated [27]. If a solvent used to create a stable suspension of ink happens not to wet the template, a second solvent that does wet the template can be used first and then replaced by the required solvent.

While this process has shown potential to become a versatile tool for sensors and printed electronics, the process still needs to be further developed and characterized before it is more widely adopted. The motivation for this work is to characterize this printing process by printing simple electronic components so that the strengths and limitations of this process can be accessed. To do this resistors, inductors, capacitors, and a simple low pass filter was made by printing silver nanoparticles using PDMS templates.

In chapter 2 models and simulations are presented for the expected behavior of the printed components. Chapter 3 details the fabrication process, and the experimental results are presented in chapter 4. Finally, chapter 5 features a conclusion and discusses future work with the AMPT nanoprinting process.

Chapter 2

Theory and Simulations of Passive Circuit Devices

2.1 Conductors

To be an effective tool for patterning printed electronic devices, AMPT must be able to produce features with consistent electrical properties that can be used for circuit design. While further work needs to be done to enable reliable printing of features with consistent properties of conductance, this work seeks to demonstrate that such printing is possible and that expected trends can be seen. When printing resistors with silver nanoparticles, the conductivity of printed devices will depend on parameters such as oxidation, fill density of printed features, and sintering which are explored below.

2.1.1 Oxidation and Fill Density

Naturally, silver tends to have an oxide thickness of 1-2 nm [35]. At standard pressure and temperature oxidation of silver happens according to the following two reactions:

$$4Ag + O_2 \longrightarrow 2Ag_2O \tag{2.1}$$

$$2Ag + O_2 \longrightarrow 2AgO \tag{2.2}$$

Due to an increased surface area to volume ratio, nanoparticles are much more susceptible to the effects of oxidation than bulk metals. To stop oxidation, metal nanoparticles are typically capped with organic stabilizers that help prevent oxidation and coalescence of nanoparticles [36]. These protective coatings are rarely 100% effective in silver and typically the silver oxidized under these layers is much greater than the defects in the protection layer. To reduce the risk of oxidation care can be exercised to limit the

exposure of silver nanoparticles to air. While the specific effects of oxidation on the conductivity of patterned silver nanoparticles are not explored through experimentation in this report, it should be seen as a complicating factor.

One problem that arises in AMPT is when that nanoparticles do not completely fill the template as a result of blockages resulting from dry out midway through a channel as illustrated in Figure 2.1. When this happens electrical conductivity of printed conductors may be greatly diminished as a result of discontinuities and reduction in cross sectional area.

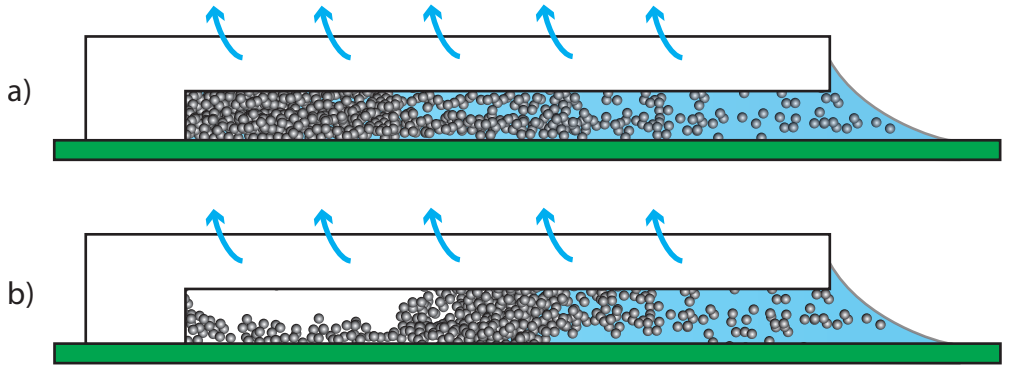

FIGURE 2.1: Channel cross section. Proper molding occurs when channels fill from the end of the channel gradually towards the front (a). Incomplete patterning occurs when when nanoparticles coalesce prior to the channel end a result of premature solvent drying (b).

2.1.2 Effect of Sintering

While nanoparticle inks allow for the printing of metals, dry nanoparticles have a low conductivity, typically more than five orders of magnitude less than that of bulk metals [37] making the conductivity of printed features void of practical importance [36]. Since the surface atoms of metal nanoparticles contain many dangling bonds, they exist with a higher surface energy than bulk metals. To reduce this surface energy, groups of nanoparticles coalesce when they come into contact.

The low conductivity of nanoparticle structures is in part due to the insulating ligand stabilizers that coat nanoparticles to help prevent oxidation. Stacking faults during coalescence and the spherical shape of nanoparticles limits electrical pathways though nanoparticle structures decreasing conductivity. Grain boundaries scatter electrons and

have been shown to increase resistivity in thin films [38]. To recover the higher conductivity of bulk metals nanoparticles need to be sintered, typically done through a high temperature annealing process.

Sintering of silver nanoparticles typically improves conductivity to 20-60% of bulk silver [39]. The sintering process of metal nanoparticles is shown in Figure 2.2. At around 165 deg C capping molecules melt or desorb, allowing for greater metal to metal contact [40]. Near the nanoparticle melting temperature, typically $\approx$ 10% of the bulk metal[41], necking begins to occur between particles as a result of diffusion of surface atoms to reduce the surface energy state causing a significant increase in conductivity[42]. Finally if the annealing process is maintained for an extended duration grain growth continues at a temperature dependent rate to further increase conductivity.

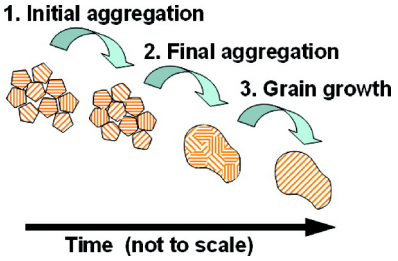

FIGURE 2.2: Steps of sintering. Capping molecules melt or desorb (1), necking occurs as a result of surface atom diffusion (2), and grain grows continues while high temperatures are maintained (3)[40]

Densification occurs during sintering as void spaces between nanoparticles are removed. This can be seen in Figure 2.3 as the porous spaces between nanoparticles disappears while annealing at a constant temperature. As a result of densification, the profiles of sintered features have a much lower height to width aspect ratios than the template they were printed from. This not only reduces the effective cross sectional area of conductors, but it increases the overall width of features potentially the cross sectional area that is used in thin-film capacitors.

2.2 Thin-Film Capacitors

Capacitors are an essential component for printed electronics as they are used for energy storage, power conditioning, signal coupling and decoupling, filtering out signal noise

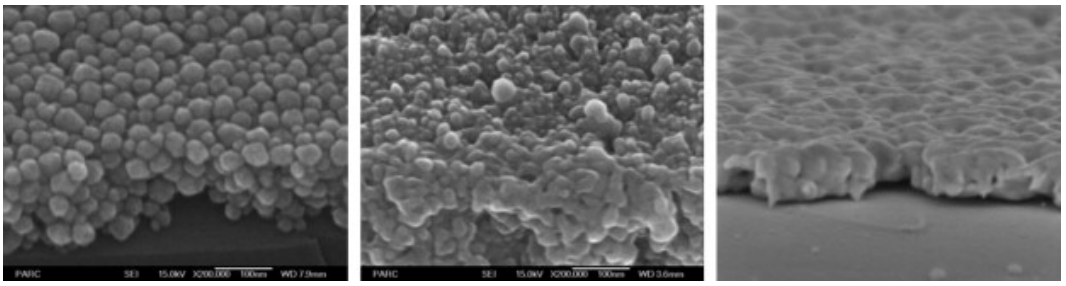

FIGURE 2.3: SEM images of 100nm silver particles as dried (left), following a 150 deg C cure for 5 minutes (center), and following a 3 hours cure (right). [41]

and sensing applications. As such, it is important to be able to easily print capacitive structures to eliminate post-printing costs of attaching stand-alone components.

Capacitance is most frequently described in terms of the two-dimensional parallel plate model.

$$C = \epsilon_0 \epsilon_r \frac{A}{d} \tag{2.3}$$

From this model it can easily be seen that maximizing capacitance is done by increasing the plate area, decreasing the cap, and using a high dielectric material between the plates. Using PMP, patterning of feature having resolutions of <350 nm have been achieved, however with the use of PDMS features are limited to $\approx 10\mu$m [43] due to the higher flexibility of the material. Since small patterns could not be printed it was determined that capacitors with interdigitated fingers, like those found comb-dive accelerometers, would be limited to picofarads and therefore unsuitable for use for practicable passive filters.

To decrease the distance between capacitive plates, it was decided to print on silicon wafers with a thin layer of silicon nitride. By doing this the capacitance was greatly increased as the gap spacing was reduced to 100 nm and a seven fold increase was had by using a dielectric layer.

While thin-film capacitors are commonly made using standard fabrication, making them using AMPT provided a set of challenges. Large parallel plate structures are typically used in thin-film capacitors, but wide structures don't pattern well using the AMPT process. If structures are too wide, the lack supporting pillared features will cause a template to collapse due to its low Young's modulus. When large areas are patterned, the template quickly becomes saturated with solvent greatly increasing the patterning time

and leading to uneven patterning. To sidestep these obstacles, the fingered capacitive structure shown in Figure 2.4 was used.

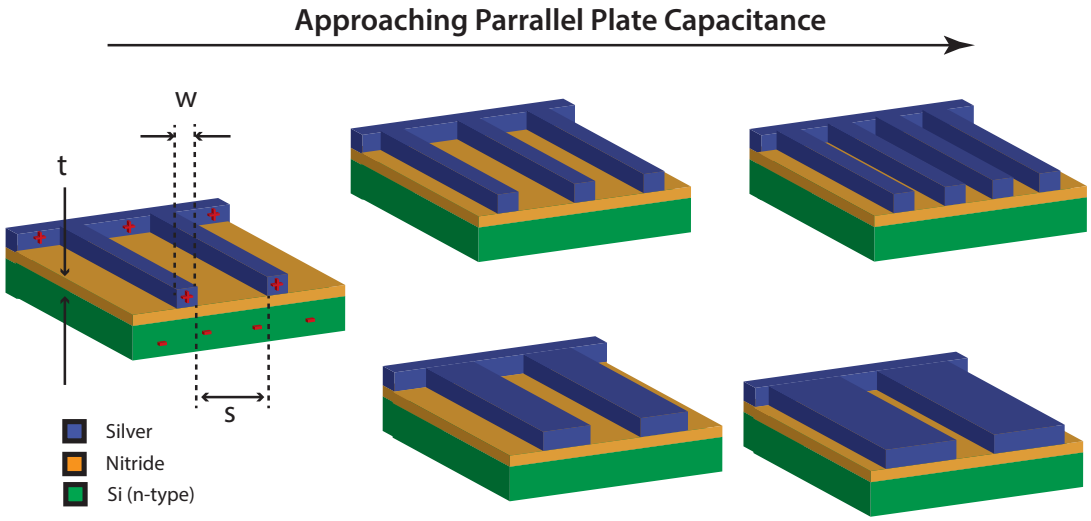

FIGURE 2.4: Fingered capacitor design lessens the potential for template collapse and slow patterning.

This fingered structure has several advantages for use with AMPT printing. First by using long straight channels the template structure is preserved during patterning and saturation of the template is less of a concern. Secondly as nanoparticle ink costs will be a driving factor in the use of AMPT printing, this fingered structure will be able to achieve equivalent capacitance to parallel plate structures while using less ink by capitalizing on the use of fringing fields.

Closed form models of fringing fields have been made [44], however these models have difficulty accounting for the geometrical constraints of repeated fingers and multiple dielectric materials such as the silicon nitride and air configuration that is found in this structure. To see the effects of the fringing fields a 2-D electrostatic model of the capacitive structure was made (Figure 2.5) from which the capacitance per unit area could be estimated for various finger widths w, spacing s, and silicon nitride thicknesses d.

As the dimensions of w and s approach d the capacitance of the fringing electric field adds significantly to the overall capacitance. This can be seen in Figure 2.6 where the effect of scaling w and s concurrently is shown. For any given values of w and d there exists a certain finger spacing that optimizes the use of fringing fields (see Figure 2.7.

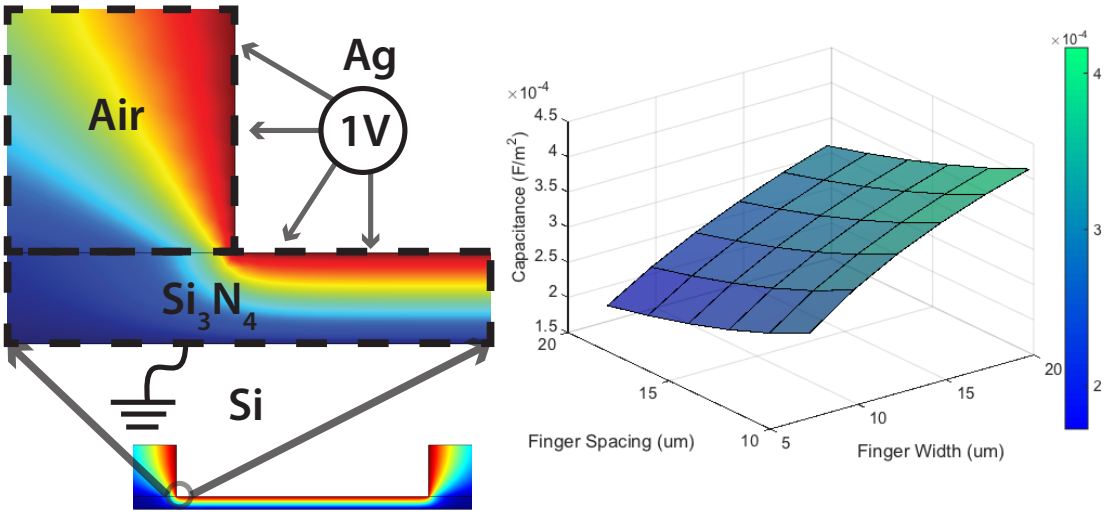

FIGURE 2.5: COMSOL was used to model the the 2-D capacitive structure. $\epsilon_r = 7.0$ for Si_3N_4. The right hand plot shows shows the expected relationship between the finger width and finger for *d=250 nm.*

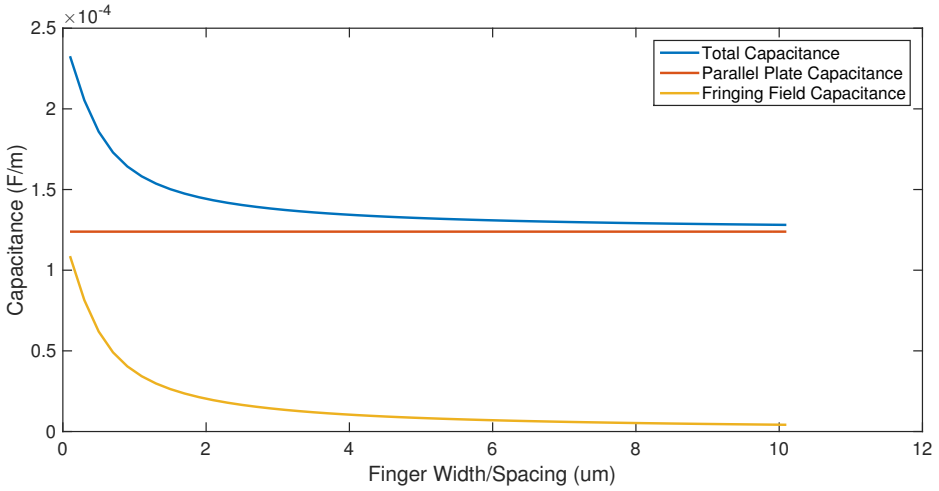

FIGURE 2.6: Capacitance as a function of concurrent scaling of w and s for d=250 nm.

2.3 Spiral Inductors

Inductors are widely used in microelectronic circuits for applications such as energy storage, intermediate frequency filters, voltage controlled oscillators, low-noise amplifiers, mixers, and sensing applications [45]. As with capacitors, the ability to print inductors is strongly preferable to using bond wires with external components to reduce costs and increase versatility.

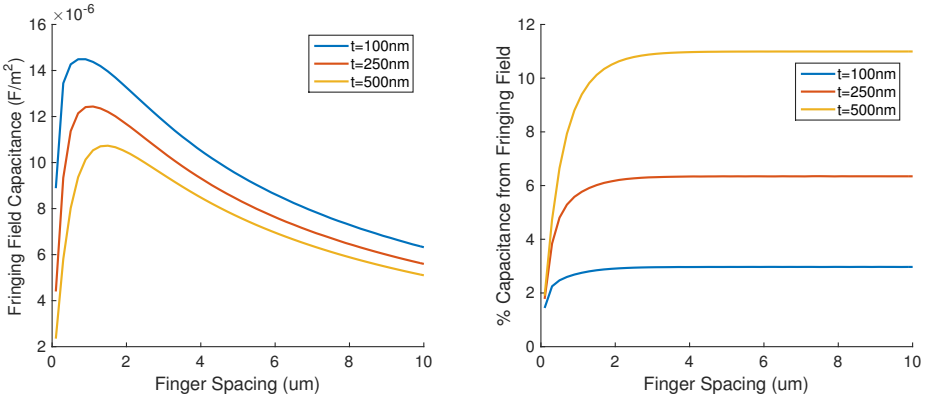

FIGURE 2.7: Simulated results for w=5. For a given w and s there exists an optimal finger spacing (left). As finger spacing is increased the benefits of fringing fields taper off (right).

While externally mounted inductor components can benefit from higher Q's, planar spiral inductors have lower Q's but are more robust to process variations[45]. To use spiral planar inductors in printed electronics, it will be necessary to print on a on a substrate with patterned conductive and insulating layers to allow for electrically isolated access to the inner inductor electrode. This is left for future work as the inductance can easily be measured using probe tips.

The two planar inductor layouts that were chosen were square spirals and an Archimedes spiral shown in (Figure 2.8) because of their common use. For each of these geometries approximate expressions for inductance, shown to have an error less than $\approx$ 5% of experimental values, have been developed by *Mohan et al.*[46]. These expressions are based on the number of turns n, the turn width w, the turn spacing s, and the average diameter $d_{avg} = 0.5(d_{out} + d_{in})$ or the fill ratio $\Delta = (d_{out} - d_{in})/(d_{out} + d_{in})$. The thickness of an inductors has a minimal effect and is typically left out of approximate expressions [47].

The first expression given in equation 2.4 has been termed the Modified Wheeler formula as it was based upon the expression Wheeler obtained for discreet inductors [48]. In this expression the coefficients K_1 and K_2 are dependent on the spiral layout (Table 2.1).

$$L_{mw} = K_1 \cdot \frac{\mu_0 n^2 d_{avg}}{1 + K_2 \Delta} \tag{2.4}$$

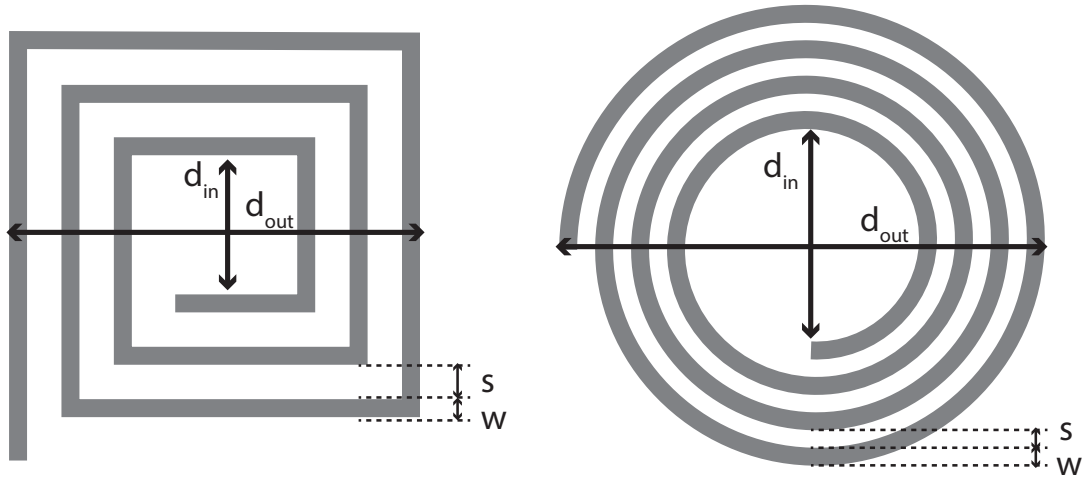

FIGURE 2.8: Layout for planar square and circular spiral inductors

TABLE 2.1: Coefficients for Modified Wheeler Expression

Layout	K_1	K_2
Square	2.34	2.75
Hexagonal	2.33	3.82
Octagonal	2.25	3.55

The second expression given in equation 2.5 and is accurate when $s \leq w$. This expression is derived by approximating the sides of a spiral as symmetrical current sheets of equivalent current densities. The coefficients c_1, c_2, c_3, c_4 are dependent on the spiral configuration (Table 2.2).

$$L_{gmd} = \frac{\mu_0 n^2 d_{avg} c_1}{2} \cdot (ln(\frac{c_2}{\Delta}) + c_3\Delta + c_4\Delta^2) \tag{2.5}$$

TABLE 2.2: Coefficients for Current Sheet Expression

Layout	c_1	c_2	c_3	c_4
Square	1.27	2.07	0.18	0.13
Hexagonal	1.09	2.23	0.00	0.17
Octagonal	1.07	2.29	0.00	0.19
Circle	1.00	2.46	0.00	0.20

2.4 Passive Low-Pass Filter

Filters are widely used to give circuits such as amplifiers, oscillators and power supply circuits a certain frequency characteristic by removing unwanted frequency components from the signal or enhancing the desired ones. Passive filters are distinguished from active filters in that they are made purely from resistors, capacitors, and inductors and do not require an active power supply to operate. Using the capacitor model previously described low-pass filters can easily be configured by patterning on a silver layer with a 100 nm silicon nitride dielectric layer as illustrated in Figure 2.9. Although not explored in this work it can also be seen that by switching the terminals, the low pass filter can easily be configured into a high-pass filter.

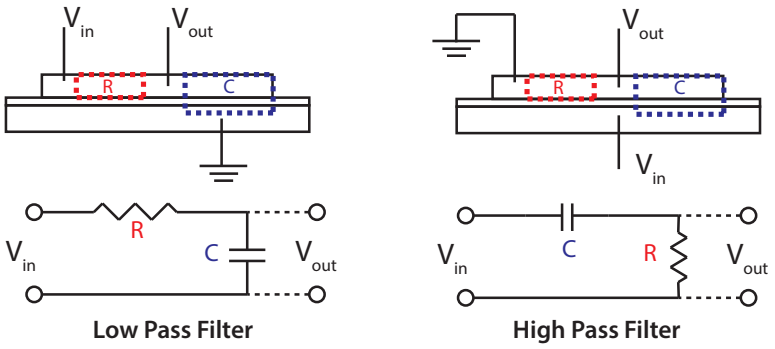

FIGURE 2.9: Configuration for low-pass and high-pass filters

Low-pass filters are commonly used to smooth signals by eliminating high frequency noise. Doing a simple voltage divider analysis of the circuit using the complex impedances the low-pass filter transfer function is easily derived (equation 2.7) having a frequency dependent magnitude (equation 2.8). Simple first order low-pass filters are typically described using a cut off or break frequency, ω_{break}, at which the input power is halved or reduced by 3 dB.

$$Z_R = R, \qquad Z_C = \frac{1}{j\omega C} \tag{2.6}$$

$$H(j\omega) = \frac{V_{out}}{V_{in}} = \frac{1}{j\omega RC + 1} \tag{2.7}$$

$$|H(j\omega)| = \sqrt{\frac{1}{1 + \omega^2 R^2 C^2}} \tag{2.8}$$

$$\omega_{break} = \frac{1}{RC} \tag{2.9}$$

Using AMPT, it would be difficult to print a low pass filter that would accurately be described by the derivation above due to parasitic capacitances along the resistor portion of the patterned features. A more accurate model of the low pass filter including the parasitic capacitance is shown in Figure 2.10. Dividing the resistor into m steps each with a resistance of R_p and capacitance of C_p the transfer function becomes:

$$H(j\omega) = [\frac{1}{j\omega R_p C_p + 1}]^m \frac{1}{j\omega RC + 1} \tag{2.10}$$

The effect of the parasitic capacitance is that the cut off frequency is increased but the roll-off attenuation is also increased. This means that the shift of ω_{break} is accounted for than the performance of the low-pass filter can be greater.

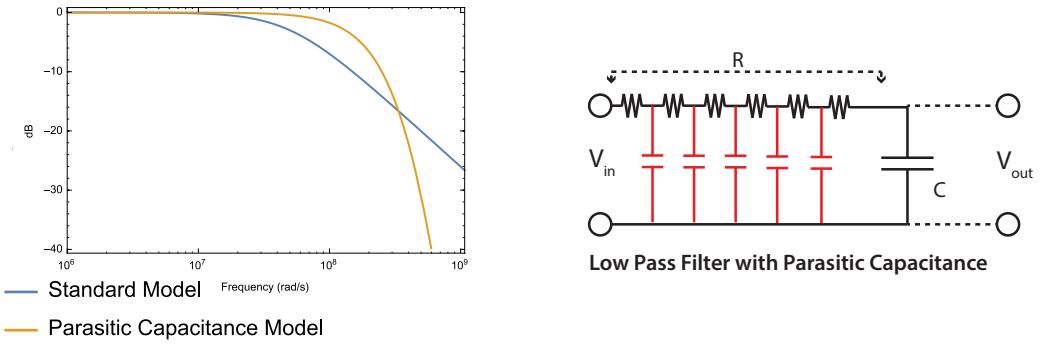

FIGURE 2.10: Parasitic capacitance in the resistor must be accounted for since no insulating layer is patterned prior to printing silver nanoparticles (right). The effect of parasitic capacitance increases its cut-off frequency and roll off. This Bode plot was made to approximate the response of one of the designed capacitors assuming $m = 10$, $\epsilon_r = 7$ and a resistivity of nearly half that of bulk silver.

Chapter 3

Fabrication Methods

3.1 Materials

AMPT printing was performed using silver nanoparticles of a mean diameter of $\approx$ 20nm suspended in an ethanol solvent. Conductors and inductors were printed on glass slides while capacitors and filters were printed on 4" silicon wafers from *MTI Corp* with 100nm and 300nm layers of Si_3N_4 deposited with low-stress PECVD.

Master molds were created from 4" silicon wafers patterned with SU-8 2015 photoresist from *MicroChem*. While the best printing resolution has been achieved with PMP templates, PDMS was chosen because of its availability, low-cost, and simplicity in casting.

3.2 Patterning Procedure

3.2.1 Creating a Master Mold

To make permeable templates a hard master mold was first made using standard photolithography (Figure 1.1) from which permeable templates were cast from. The 2D geometry was designed using *Tanner EDA's L-Edit* layout editor. A dark field 1.25μm mylar photomask was purchased from *CAD Art Services Inc.*

Silicon wafers were solvent cleaned by 5:00 ultrasonic washes in acetone and in IPA followed by a 5:00 rinse in DI water. A dehydration bake of wafers was performed at 95°C for 10:00 to promote the adhesion of photoresist to the substrate. SU-8 was then spin casted onto the wafers using a spin speed of 500RPM with an acceleration of 100RPM for 30 seconds, followed by 3500RPM with an acceleration of 300RPM for 30 seconds. Following spin casting, a soft bake was performed at 95°C for 2:45

to remove photoresist solvent. An OAI Series 200 Aligner was then used to expose the substrate at with an energy density of $130mJ/cm^2$ to crosslink photoresist in the locations defined by the photomask. SU-8 developer was then used to selectively remove the uncrosslinked photoresist, and a hard bake was performed to further solidify the pattern of the remaining photoresist. Using a Veeco Dektak 3030 profilometer several measurements of the resist layer were taken showing good height uniformity of $10.0 \pm .15\mu m$.

To aid in the removal of PMDS templates cast of these SU-8 masters a Teflon coating was deposited. To do this the masters were treated with surface-treated by trichloro (1H,1H,2H,2H-perfluorooctyl) silane (97%, Sigma-Aldrich, USA), which is also called PFOCTS. The treatment was carried out in an encapsulated chamber under a pressure of about -0.5 bar to deposit a thin layer of PFOCTS onto the surface of the mold.

3.2.2 Casting a Template

To prepare for casting PDMS (Sylgard 184 - Dow) prepolymer and cross-linker were mixed in a 10:1 ratio. To remove suspended air bubbles, the mixed solution was subjected to 3 pump downs in a low-pressure chamber. Aluminum foil was then wrapped around the master molds created a container. PDMS was poured over the master molds to a thickness of ≈ 0.5" and the system was left on a hotplate at $70°C$ overnight to cure.

Once cured, the PDMS was pealed back from the silicon and cut with a razor blade to separate the various templates made on a single wafer and to provide access to the template channels.

When preparing a previously used template for printing, scotch tape was used to remove the majority of nanoparticles from the surface of the template. Templates were then sonicated for 10 minutes in IPA and dried with nitrogen.

3.2.3 Printing

The press used for printing is shown in Figure 3.2. The press consisted of a moving platform, a heated spring stage, and an acrylic top plate. Once a template was cleaned and prepared, it was attached to the upper acyclic top plate by using van der Waals

forces. The substrate was then placed on the heated stage which was regulated at $45 \pm 5°C$ to increase solvent evaporation, and the stage was raised until the top of the substrate was nearly in contact with the template. A this point a syringe containing methanol with no nanoparticles was used to apply solvent to the substrate until it formed a large meniscus around the template edges. The stage was then raised until a small deformation in the side profile of the template was observed, verifying that the template was in good contact with the substrate. To ensure an even pressure distribution could be gradually applied to the template the spring stage was needed to automatically correct for any error in parallelism of the template and the substrate. Shortly after making contact, any residual methanol trapped under the template in regions where it should be excluded was evaporated leaving no residual layer behind.

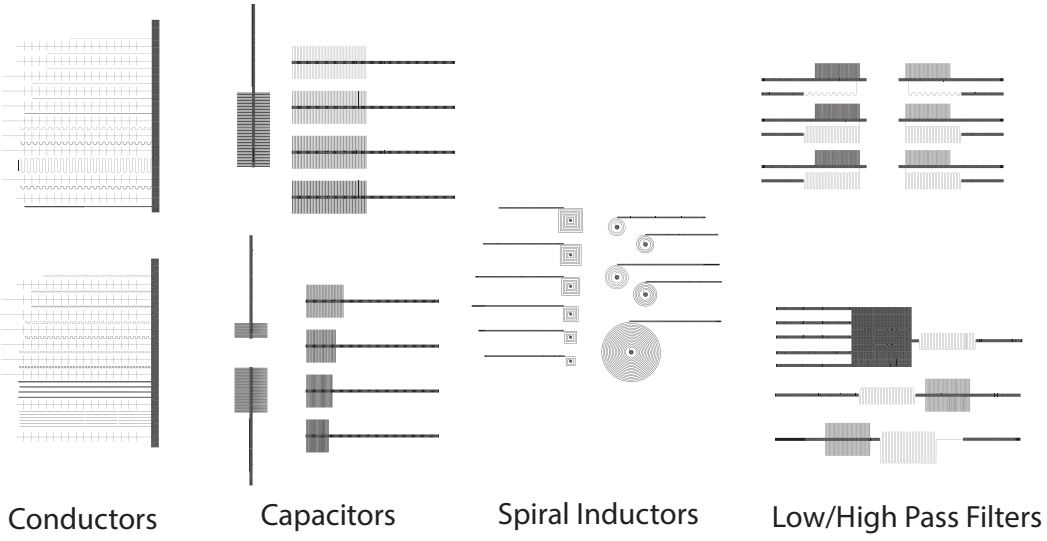

FIGURE 3.1: 2D geometry was created in *L-Edit* to and patterned onto a dark-field mask. Here features are colored black for clarity, however the mask has an inverted color scheme with transparent features and a black background.

Having prefilled the template with solvent, nanoparticle ink was deposited along the solvent meniscus near the channel openings in the template. As the ethanol evaporated through the template, the ink was drawn into the channels where the nanoparticle concentration condensed as the solvent evaporates. To prevent gasses entering the channels, which would stop the patterning process, additional solvent and nanoparticle ink was routinely added to maintain a meniscus along the edge of the template. As the nanoparticles concentrated in the channel a color change of clear to yellow and finally to a dark gray was observed. Once channels were filled, the addition of solvent to the

template edge was stopped and any remaining solvent amid the condensed nanoparticles was allowed to evaporate leaving only the dried nanoparticles.

Having completed the printing process the stage was lowered and the PDMS template was removed from the substrate. Since the remaining solvent had been evaporated, reflow of ink on the surface of the substrate was prevented and features maintained their original geometry. Nanoparticle features were then sintered for ≈30 minutes at $250 \pm 5°C$ after which a second color change from dark gray to a traditional silver color was observed.

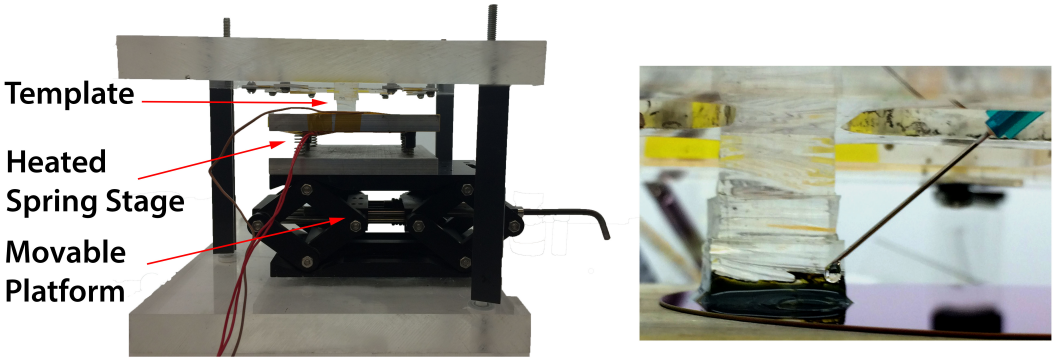

FIGURE 3.2: The press used from patterning inks consisted of a moving platform and a heated spring stage to ensure an even pressure distribution on the template. The continual addition of solvent is necessary to prevent premature dry out in channels.

Chapter 4

Characterization of Printed Devices

4.1 Conductors

To characterize conductors using AMPT, straight and meandering conductive traces printed (see Table‘4.1), a few of which are shown in Figures 4.1 and 4.7 to measure the range in resistance and conductive uniformity that could be expected from typical features. Measurements were taken along the $500\mu m$ markings, indicated by vertical "tick" makers seen in the images using a Probe station configured to an Aligent E4980A LCR meter. While measurements generally appeared to increase with respect to longer lengths and narrower widths, measurements were highly inconsistent. When re-measuring the same segment multiple times by lifting a probe tip and lowering it back into contact, measurements would fluctuate be between $\approx 1\Omega - 1M\Omega$ suggesting poor contact between the probe tip and the patterned silver. When leaving the probes in contact with the features it was also observed that measured values would increase over time. Two likely scenarios for this would be that the silver features were increasing in temperature due to the DC voltage required for measurement, or that there was a problem with the configuration or compensation procedure of the LCR meter.

Table 4.1: Conductive traces that were printed

Trace Layout	Width (μm)	Length (cm)
Straight lines	7, 10, 15, 20, 25, 30, 40, 50	≥ 0.7
Square waves	10, 15, 20	≥ 1.4
Triangle waves	10, 15, 20	≥ 1
Sine waves	10, 15, 20	≈ 2.1
Stretched - Sine wave	10	> 4

Figure 4.2 depicts proper filling of channels that fill from the from the end of the channel first. While this difference can easily be seen in images after devices have been printed and sintered, it is difficult to observe during the printing process. Due to the inability to achieve reliable resistance measurements it was difficult to make numerical conclusions

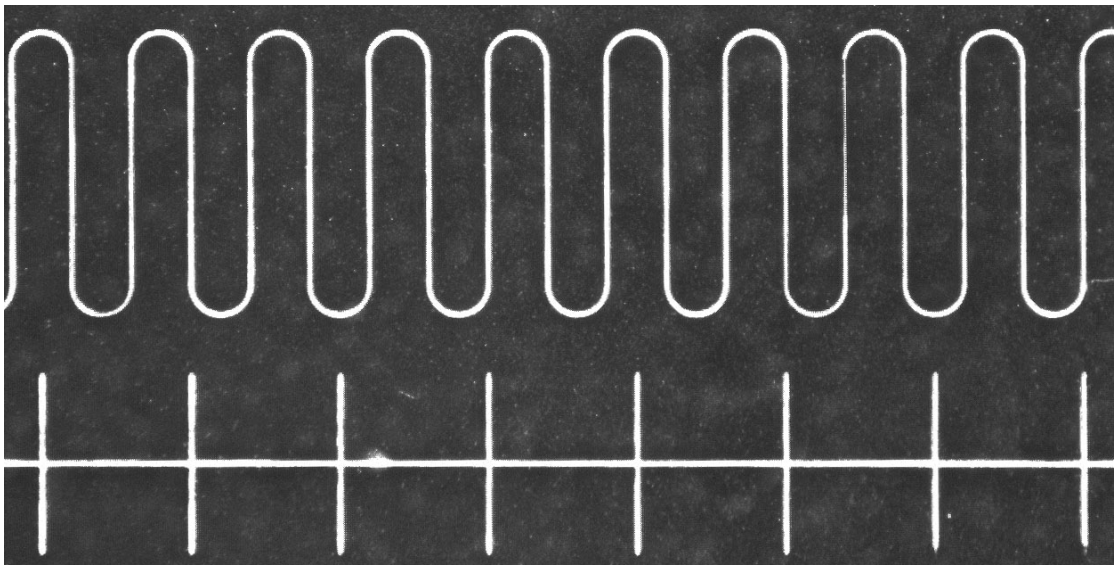

FIGURE 4.1: Serpentine channels, used to increase the overall length, were able to be patterned with good fidelity. Vertical "tick" marks are spaced $500\mu m$ apart.

about the consistency of the resistance in the printed silver features across a printed device. Measurements less than 10Ω, if accurate, however would indicate that good electrical connections are easily achievable.

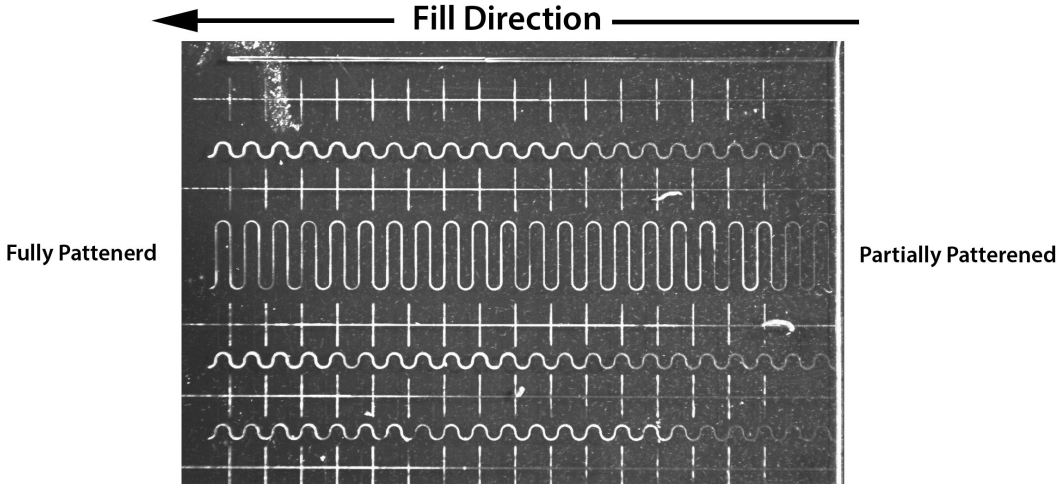

FIGURE 4.2: Concentration of nanoparticles first occurs at the end of the channels. The right hand side of the image, near the channel inlets, shows features that are much more transparent on the glass substrate indicating that only partial patterning occurred. Channel widths shown in this image are $10\mu m$,$15\mu m$, and $20\mu m$. Vertical "tick" marks are spaced $500\mu m$ apart.

4.2 Thin-Film Capacitors

Thin film capacitors were printed on silicon wafers with $100\mu m$ and $300\mu m$ of silicon nitride (listed in Table 4.2). Unlike the conductors that were printed on glass, nanoparticles printed on silicon nitride were easily damaged or completely removed when separating the template after printing. Due to the poor adhesion of silver nanoparticles to the silicon nitride surface most of printed capacitive structures were completely destroyed upon template removal. Figure 4.3 shows the three capacitive structures that were characterized. Figure 4.4 shows a detailed image of the most successfully printed capacitive structure.

TABLE 4.2: Specifications of printed thin-film capacitors

w (μm)	s (μm)	t (nm)	Finger length (mm)	# of Fingers
10	10, 20, 30, 40, 50, 90	100,300	1	100
20	80	100,300	1	100
30	70	100,300	1	100
40	60	100,300	1	100
50	50	100,300	1	100

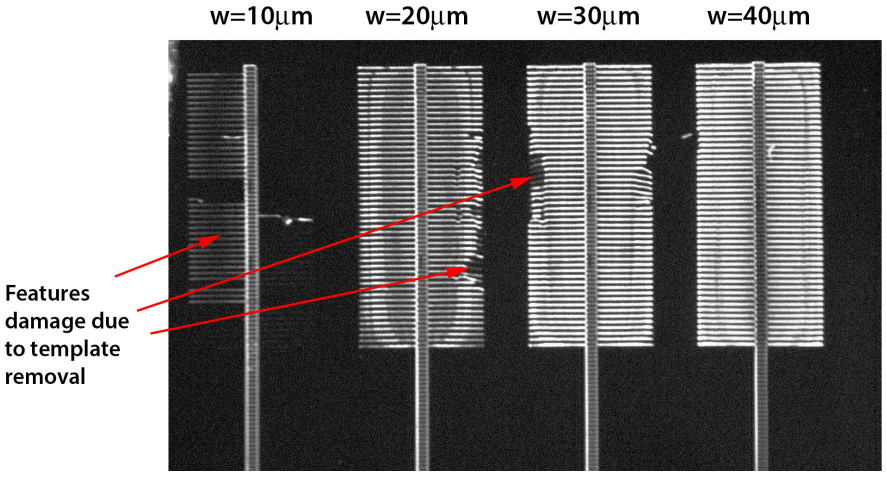

FIGURE 4.3: Fingered capacitors were printed of varying finger widths.

To characterize the capacitive devices a probe station configured to an Agilent B1500A Semiconductor Device Analyzer was used. As shown in Figure 4.5, frequency sweeps were conducted between 1kHz and 1MHz for each structure. Since the impedance of a capacitor is $Z = \frac{1}{j\omega C}$, the roll of in capacitance observed at higher frequencies is expected as a the capacitor transitions from performing as a open circuit to a short

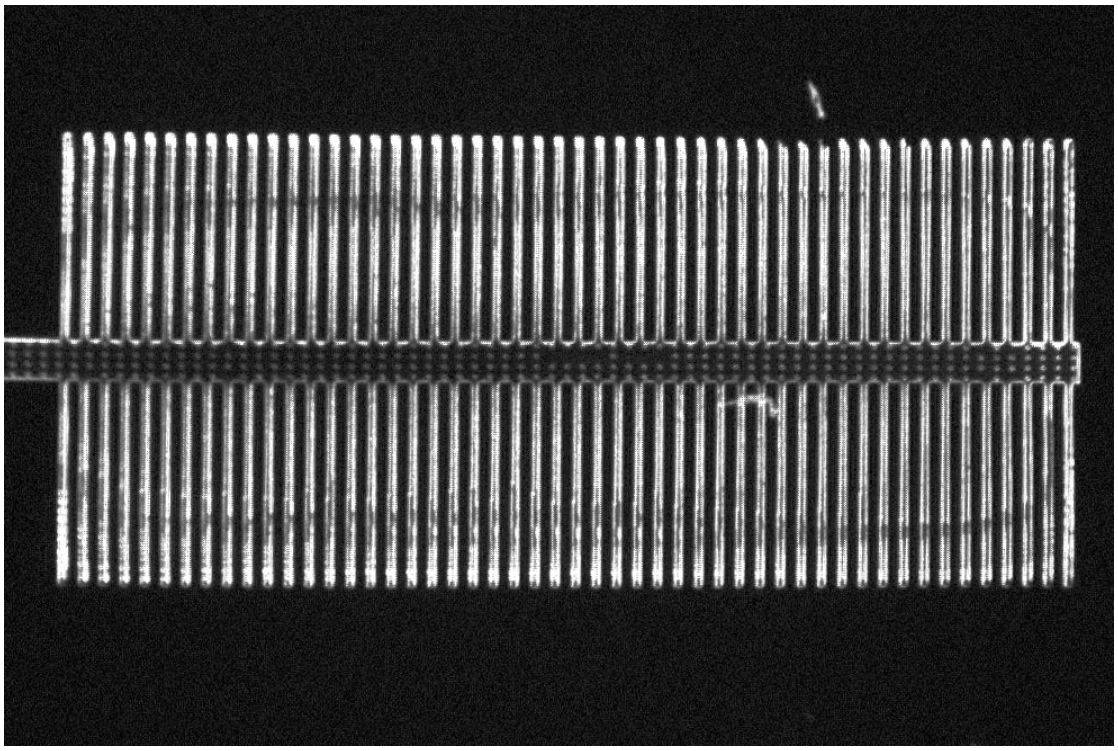

FIGURE 4.4: An enlarged image of the capacitor with $w = 40\mu m$

circuit. The roll-off location is determined by the both the resistance and capacitance of the device. The capacitor with $20\mu m$ finger widths likely rolls off much sooner as it appears to have not not fully patterned and likely had a higher resistance. As show in Table 4.3 measured low frequency capacitance was close to the that which would be approximated by the parallel plate approximation differing by less than a factor of two. As discussed in Chapter 2, the fringing fields only become significant as ω approaches d leaving this effect unobserved in the tested devices.

TABLE 4.3: Expected and measured capacitance values

	Parallel Plate Approximation (nF)	Low Frequency Measurement (nF)
$w = 20\mu m$	1.24	1.2
$w = 30\mu m$	1.86	1.42
$w = 40\mu m$	2.48	1.44

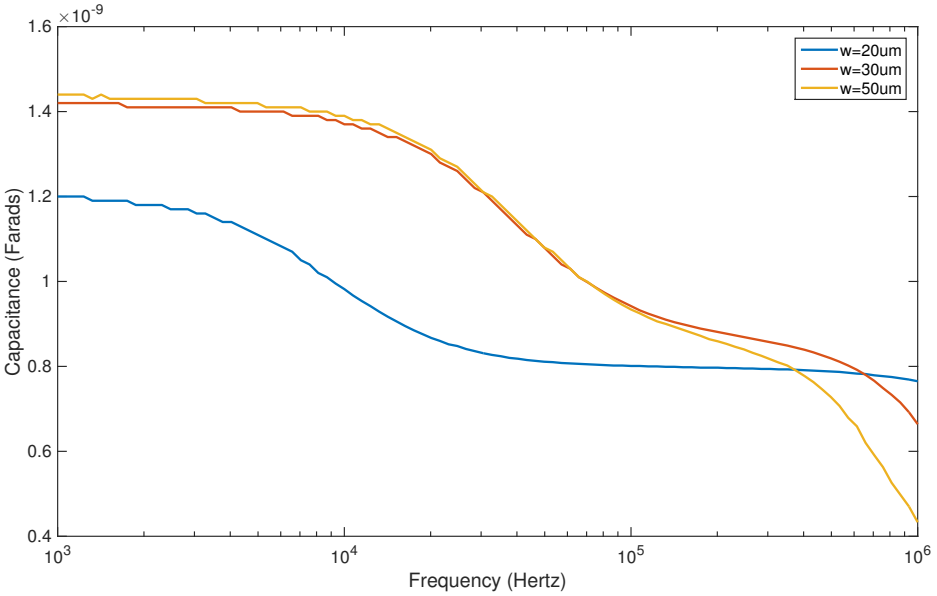

FIGURE 4.5: The Capacitance frequency response for the three well patterned structures shown in Figure 4.3

4.3 Spiral Inductors

Square and circular spiral inductors (listed in Table 4.4) such as the one showed in Figure 4.6 were successfully printed. Using the approximate inductance expression given in equation 2.5, the inductor of Figure 4.6 was expected to have a measurement of $535 \pm 54\mu H$. Unfortunately due to difficulties experienced with the configuration of the probe station and LCR meter, previously described, reliable measurements were not achieved.

TABLE 4.4: Specifications of printed spiral inductors

Layout	w (μm)	s (μm)	n	d_{in} (μm)
Square	20	80	2, 3, 4, 5, 6, 7	500
Circle	20	80	3, 5, 16	600
Circle	10	80	3, 5	

4.4 Analysis of Results

Prior to this work, AMPT had only been used to demonstrate straight features for test structures [43] and gas sensing [9]. It was unclear if inconsistent patterning would result

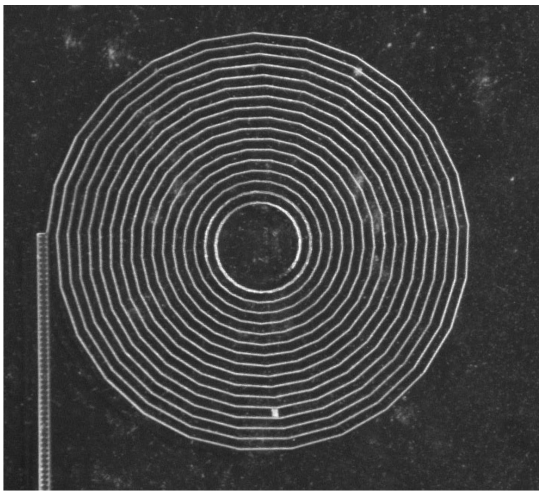

FIGURE 4.6: A well-patterned spiral inductor. A blockage appears to have stopped the innermost spirals from filling, however this is still the longest channel successfully printed to date.

due to paths with sharp bends or right angles. In observations from printed devices as those shown in Figures 4.2,4.1, 4.1 channels featuring bends did not appear to suffer from blockages or premature dry out.

The main difficulty in AMPT as it is currently performed is that it is a very non-standardized process. The ability to achieve a high quality patterning is an art as the effect of factors such as temperature, template contact pressure, and nanoparticle ink to solvent concentrations are largely unknown and these parameters are poorly monitored. As seen in Figure 4.7, applying too much pressure to the template can result in channel collapse and some features not being patterned, while to little pressure can result in separation of the template and an unwanted residual layer as seen in Figure 4.8. While the heated spring stage temperature was regulated using a thermocouple temperature swings of $\approx 10°C$ were observed, significantly affecting the solvent evaporation rate. The most difficult parameter to control is the nanoparticle concentration, which is done by adding pure solvent or the ink with a syringe during the printing process. Ideally a high nanoparticle concentration is desired to reduce the patterning time, however a high concentration of nanoparticles appears to be correlated more instances of dry out and blocked channels.

Another observation that was observed is that the density of patterned structures greatly affected the filling time. Capacitive structures such as those in Figure 4.3 took nearly three hours to fill. This can be seen visually by the parabolic lines seen when looking

across the fingers near their base. In contrast, many of the test structures used for conductivity characterization fully patterned in 30 minutes or less. Occasionally patterning would appear to halt for a prolonged period of time before suddenly progressing very quickly suggesting that a blockages had formed and then cleared. If the speed of patterning is to be increased, a solution that would allow evaporation through the top of the template needs to be made. Allowing for the solvent evaporation would also allow for increased feature density as complete template saturation would be less significant. One possible way this could be achieved would be by replacing the acrylic top plate on the press with a rigid mesh that would allow for more rapid escape of solvent into the surrounding air.

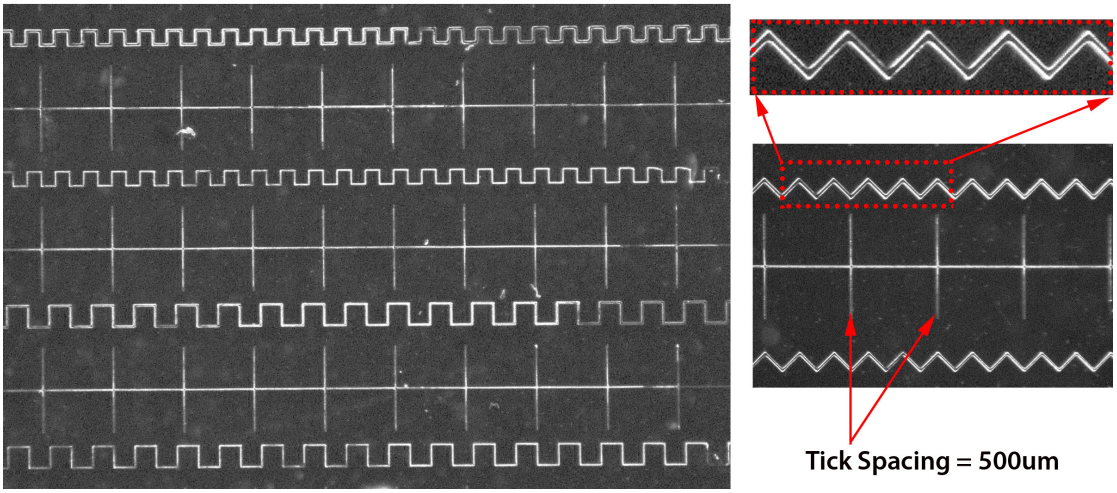

FIGURE 4.7: Along with being able to pattern straight channels and serpentine channels, square-wave and saw-tooth channels were patterned successfully. Occasionally features only appeared to have patterned near the feature edge indicating a channel collapse during patterning.

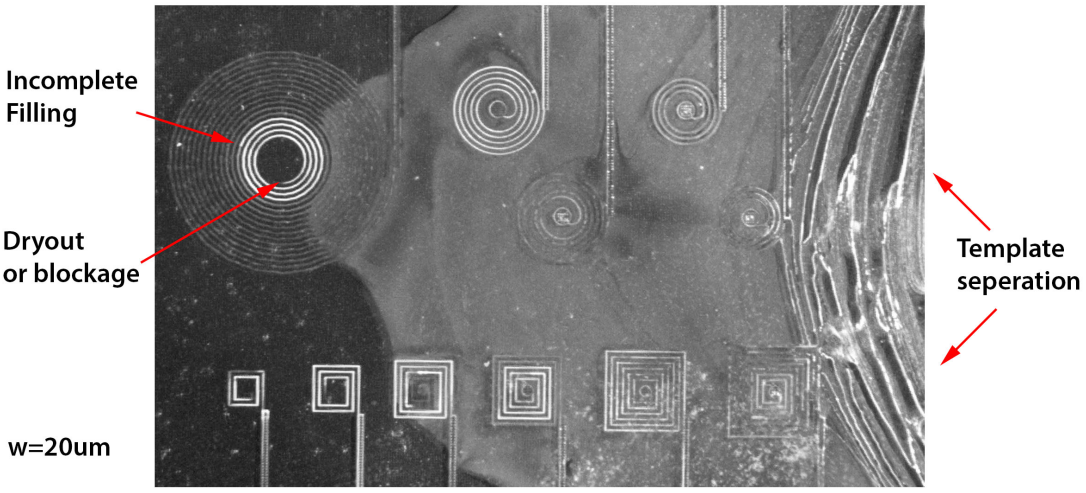

FIGURE 4.8: Applying too little pressure on the template resulted in separation from the substrate and an unwanted residual layer.

Chapter 5

Conclusion

5.1 Summary

In this report models for the expected performance of the most frequently used passive electrical components in microelectronics were presented. Prior to this work, AMPT had only been used to produce straight features and it was unclear if the geometries of conductors, capacitors, and inductors would pattern properly. These devices were successfully printed demonstrating that AMPT is capable for a printing all the necessary components for printed sensors and electronics. While complete characterization of conductors and inductors was not achieved, all results that were obtained were in alignment with the models presented. Lastly, fingered thin-film capacitors were tested and shown to have capacitances close to expected values.

5.2 Prospective Uses for AMPT

Providing AMPT can be developed into a roll-to-roll printing process it may become cost advantageous to use for a number of commercial applications that currently use traditional and alternative fabrication methods. Since printing is done using low temperatures and pressures AMPT should allow for printing on flexible and delicate substrates that would not survive other printing methods.

By printing with nanoparticles and polymers AMPT may prove to be extremely useful in the manufacture of biosensors [6]Luo:2006cq., catalysts [7], photonics [8], low temperature metal electrode deposition, , gas sensors [9], and other MEMS applications [10].

5.3 Future Work

5.3.1 Sintering Characterization

As described in chapter 2, scattering greatly affects the conductivity of nanoparticles. When sintering by means of a thermal anneal, the conductivity is highly dependent on anneal temperature as well as the time the device is annealed for [41]. Along with seeing how different anneals affect the conductivity of printed nanoparticles, it would be useful to characterize how the profile of features change as a result of thermal sintering by using atomic force microscopy measurements. It is expected that there will be a trade off between annealing temperature and duration on the profile of printed features, but this is still largely unknown.

While thermal annealing is the most straight forward method of sintering nanoparticles, recent work has been done on laser sintering [49], electrical sintering [37], microwave sintering [39] of nanoparticles, and sintering at room temperature using charged poly-electrics to [36]. These methods of sintering have demonstrated as sintering of metal nanoparticles using lower or localized temperatures and shorter durations compared to thermal annealing. Demonstrating the use of these sintering methods with AMPT may make this printing process even more appealing to users who wish to print conductive metal features as the can potentially increase the versatility and decrease processing time.

5.3.2 Printing Parameter Dependency

As discussed previously, AMPT is currently non-standardized leading to inconsistent results between process runs. If AMPT is to become widely adopted, work needs to be done to determine the effects of temperature, nanoparticle concentration, template pressure, and template dimensions for various materials and solvents so that guesswork can be taken out of the printing process.

5.3.3 Printing Limitations

Once established metrics can be easily followed for optimal patterning conditions it would then be advantageous to determine design guidelines for what geometry can be printed using AMPT. Metrics for allowable channel aspect ratios, channel lengths, and feature density are all important when taking when designing features to be patterned with this process.

5.3.4 Printing on Flexible Substrates

Lastly, future work will focus on demonstrating printing on films made from materials such as polyester, polyethylene napthalate, polyimide, and various fluropolymers. AMPT may allow patterning on many of materials that pattern poorly or are incompatible with other printing processes. Work will also seek to achieve simultaneous printing on two sides of a substrate such that spiral inductors, and capacitors, and complex analog circuits can be printed in a one step process that could eventually be developed into a roll-to-roll high throughput patterning process.

Bibliography

[1] Michael T Demko, Jim C Cheng, and Albert P Pisano. High-Resolution Direct Patterning of Gold Nanoparticles by the Microfluidic Molding Process. *Langmuir*, 26(22):16710–16714, November 2010.

[2] D Senturia Stephen. Microsystem design, 2001.

[3] Banqiu Wu and Ajay Kumar. Extreme ultraviolet lithography: A review. *Journal of Vacuum Science & Technology B*, 25(6):1743–1761, November 2007.

[4] Adam Winkleman, Raquel Perez-Castillejos, Michal Lahav, Max Narovlyansky, Leonard N J Rodriguez, and George M Whitesides. Patterning micron-sized features in a cross-linked poly(acrylic acid) film by a wet etching process. *Soft Matter*, 3(1):108–116, December 2006.

[5] A P Alivisatos. *Perspectives on the Physical Chemistry of Semiconductor Nanocrystals*, volume 100. American Chemical Society, August 1996.

[6] Paul Alivisatos. The use of nanocrystals in biological detection. *Nature Biotechnology*, 22(1):47–52, January 2004.

[7] Masatake Haruta. Catalysis of Gold Nanoparticles Deposited on Metal Oxides. *CATTECH*, 6(3):102–115, 2002.

[8] Hideyuki Nakanishi, Kyle J M Bishop, Bartlomiej Kowalczyk, Abraham Nitzan, Emily A Weiss, Konstantin V Tretiakov, Mario M Apodaca, Rafal Klajn, J Fraser Stoddart, and Bartosz A Grzybowski. Photoconductance and inverse photoconductance in films of functionalized metal nanoparticles. *Nature*, 460(7253):371–375, July 2009.

[9] K L Dorsey, D A Rolfe, G D Hoople, and A P Pisano. Functionalized micromolded nanoparticles towards gas sensor arrays. *SENSORS, 2014 IEEE*, pages 1344–1347, 2014.

[10] Sawyer B Fuller, Eric J Wilhelm, and Joseph M Jacobson. Ink-jet printed nanoparticle microelectromechanical systems. *Microelectromechanical Systems, Journal of*, 11(1):54–60, February 2002.

[11] T C Pearce, J W Gardner, and S Friel. *Machine olfaction: intelligent sensing of odours*. IEEE, 1993.

[12] C Liu. Recent Developments in Polymer MEMS. *Advanced Materials*, 19(22): 3783–3790, November 2007.

[13] Brian Derby. Inkjet Printing of Functional and Structural Materials: Fluid Property Requirements, Feature Stability, and Resolution. *dx.doi.org*, 40(1):395–414, July 2010.

[14] Yeon Hee Yun, Jae Dong Kim, Byung Kook Lee, Yong Woo Cho, and Hee Young Lee. Polymer inkjet printing: Construction of three-dimensional structures at micro-scale by repeated lamination. *Macromolecular Research*, 17(3):197–202, 2009.

[15] Chieh Chang, Kevin Limkrailassiri, and Liwei Lin. Continuous near-field electrospinning for large area deposition of orderly nanofiber patterns. *Applied Physics Letters*, 93(12):123111, September 2008.

[16] N Kapur, R Hewson, P A Sleigh, J L Summers, H M Thompson, and S J Abbott. A Review of Gravure Coating Systems. July 2011.

[17] Dania A Alsaid, Erika Rebrosova, Margaret Joyce, Marian Rebros, M Atashbar, and Bradley Bazuin. Gravure Printing of ITO Transparent Electrodes for Applications in Flexible Electronics. *Display Technology, Journal of*, 8(7):391–396, July 2012.

[18] Dae-Young Chung, Dong-Seok Leem, Donal D C Bradley, and Alasdair J Campbell. Flexible multilayer inverted polymer light-emitting diodes with a gravure contact printed Cs2CO3 electron injection layer. *Applied Physics Letters*, 98(10):103306, March 2011.

[19] D Sung, A de la Fuente Vornbrock, and Vivek Subramanian. Scaling and Optimization of Gravure-Printed Silver Nanoparticle Lines for Printed Electronics. *Components and Packaging Technologies, IEEE Transactions on*, 33(1):105–114, 2010.

[20] M Hambsch, K Reuter, M Stanel, G Schmidt, H Kempa, U Fügmann, U Hahn, and A C Hübler. Uniformity of fully gravure printed organic field-effect transistors. *Materials Science and Engineering: B*, 170(1-3):93–98, June 2010.

[21] M Härting, J Zhang, D R Gamota, and D T Britton. Fully printed silicon field effect transistors. *Applied Physics Letters*, 94(19):193509, May 2009.

[22] Laura Gonzalez-Macia, Aoife Morrin, Malcolm R Smyth, and Anthony J Killard. Advanced printing and deposition methodologies for the fabrication of biosensors and biodevices . *Analyst*, 135(5):845–867, 2010.

[23] R Xu, A Lei, C Dahl-Petersen, K Hansen, M Guizzetti, K Birkelund, E V Thomsen, and O Hansen. Screen printed PZT/PZT thick film bimorph MEMS cantilever device for vibration energy harvesting. *Sensors and Actuators A: Physical*, 188: 383–388, December 2012.

[24] M Galiazzo, V Furin, D Tonini, G Cellere, and A Baccini. *Galiazzo: Double printing of front contact Ag in... - Google Scholar*. Proceedings of the 25th . . . , 2010.

[25] D H Lee, J S Choi, H Chae, C H Chung, and S M Cho. Screen-printed white OLED based on polystyrene as a host polymer. *Current Applied Physics*, 9(1):161–164, January 2009.

[26] Qiangfei Xia, Keith J Morton, Robert H Austin, and Stephen Y Chou. Sub-10 nm Self-Enclosed Self-Limited Nanofluidic Channel Arrays. *Nano letters*, October 2008.

[27] M T Demko. High Resolution Additive Patterning of Nanoparticles and Polymers Enabled by Vapor Permeable Polymer TemplatesByMichael Thomas DemkoA dissertation submitted in partial satisfaction of the requirements for the degree ofDoctor of PhilosophyinEngineering - Mechanical Engineeringin theGraduate Divisionof theUniversity of California, BerkeleyCommittee in charge:Professor Albert P. Pisano, Chair Professor Liwei Lin Professor Ming C. WuSpring, 2012. pages 1–177, April 2012.

[28] E Menard, M A Meitl, Y Sun, J U Park, and DJL Shir. Micro-and nanopatterning techniques for organic electronic and optoelectronic systems. *Chemical . . .* , 2007.

[29] Jessamine Ng Lee, Cheolmin Park, , and George M Whitesides. Solvent Compatibility of Poly(dimethylsiloxane)-Based Microfluidic Devices. *Analytical Chemistry*, 75(23):6544–6554, October 2003.

[30] Y S Kim, Joonhyung Park, and Hong H Lee. Three-dimensional pattern transfer and nanolithography: modified soft molding. *Applied Physics Letters*, 81(6):1011–1013, August 2002.

[31] I Park, S H Ko, H Pan, C P Grigoropoulos, A P Pisano, J M J Fréchet, E S Lee, and J H Jeong. Nanoscale Patterning and Electronics on Flexible Substrate by Direct Nanoimprinting of Metallic Nanoparticles. *Advanced Materials*, 20(3): 489–496, February 2008.

[32] S K Donthu, Z Pan, and G S Shekhawat. Near-field scanning optical microscopy of ZnO nanopatterns fabricated by micromolding in capillaries. *Journal of applied ...*, 2005.

[33] RNA Prebiotic. Polymer microstructures formed by moulding in capillaries. *Nature*, 1995.

[34] Alexander Blümel, Andreas Klug, Sabrina Eder, Ullrich Scherf, Erik Moderegger, and Emil J W List. Micromolding in capillaries and microtransfer printing of silver nanoparticles as soft-lithographic approach for the fabrication of source/drain electrodes in organic field-effect transistors. *Organic electronics*, 8(4):389–395, August 2007.

[35] A Rooij. The Oxidation of Silver by Atomic Oxygen. 13:1–20, August 1999.

[36] S Magdassi, M Grouchko, O Berezin, and A Kamyshny. Triggering the sintering of silver nanoparticles at room temperature. *ACS nano*, 2010.

[37] Mark L Allen, Mikko Aronniemi, Tomi Mattila, Ari Alastalo, Kimmo Ojanperä, Mika Suhonen, and Heikki Seppä. Electrical sintering of nanoparticle structures. *Nanotechnology*, 19(17):175201, April 2008.

[38] Tik Sun, Bo Yao, Andrew P Warren, Katayun Barmak, Michael F Toney, Robert E Peale, and Kevin R Coffey. Dominant role of grain boundary scattering in the resistivity of nanometric Cu films. *Physical Review B*, 79(4):041402, January 2009.

[39] Jolke Perelaer, Robin Jani, Michael Grouchko, Alexander Kamyshny, Shlomo Magdassi, and Ulrich S Schubert. Plasma and Microwave Flash Sintering of a Tailored Silver Nanoparticle Ink, Yielding 60Foils. *Advanced Materials*, 24(29):3993–3998, August 2012.

[40] Bridget Ingham, Teck H Lim, Christian J Dotzler, Anna Henning, Michael F Toney, and Richard D Tilley. How Nanoparticles Coalesce: An in Situ Study of Au Nanoparticle Aggregation and Grain Growth. *Chemistry of ...*, June 2011.

[41] Julia R Greer and Robert A Street. Thermal cure effects on electrical performance of nanoparticle silver inks. *Acta Materialia*, 55(18):6345–6349, October 2007.

[42] Teck H Lim, David McCarthy, Shaun C Hendy, Kevin J Stevens, Simon A Brown, and Richard D Tilley. Real-Time TEM and Kinetic Monte Carlo Studies of the Coalescence of Decahedral Gold Nanoparticles. *ACS nano*, 3(11):3809–3813, October 2009.

[43] Michael T Demko, Jim C Cheng, and Albert P Pisano. Rigid, Vapor-Permeable Poly(4-methyl-2-pentyne) Templates for High Resolution Patterning of Nanoparticles and Polymers. *ACS nano*, 6(8):6890–6896, August 2012.

[44] S Chowdhury, M Ahmadi, and W C Miller. A closed-form model for the pull-in voltage of electrostatically actuated cantilever beams. *Journal of Micromechanics and Microengineering*, 15(4):756–763, April 2005.

[45] M Zolog, D Pitica, and O Pop. Characterization of Spiral Planar Inductors Built on Printed Circuit Boards. *Electronics Technology, 30th International Spring Seminar on*, pages 308–313, 2007.

[46] Sunderarajan S Mohan, Maria Del Mar Hershenson, Stephen P Boyd, and Thomas H Lee. Simple accurate expressions for planar spiral inductances. *Solid-State Circuits, IEEE Journal of*, 34(10):1419–1424, October 1999.

[47] Goran Stojanović, Ljiljana Živanov, and Mirjana Damnjanović. Optimal design of circular inductors. *Facta universitatis - series: Electronics and Energetics*, 18(1): 57–70, 2005.

[48] H A Wheeler. Simple Inductance Formulas for Radio Coils. In *Radio Engineers, Proceedings of the Institute of*, pages 1398–1400. IEEE, 1928.

[49] Seung Hwan Ko, Jaewon Chung, Heng Pan, Costas P Grigoropoulos, and Dimos Poulikakos. Fabrication of multilayer passive and active electric components on polymer using inkjet printing and low temperature laser processing. *Sensors and Actuators A: Physical*, 134(1):161–168, February 2007.